Shear, compressive and dilatational response of rubberlike solids subject to cavitation damage

A. Dorfmann, K.N.G. Fuller, R. W. Ogden

Shear, compressive and dilatational response of rubberlike solids subject to cavitation damage

A. Dorfmann [a,*], K.N.G. Fuller [b], R.W. Ogden [c]

[a] *Institute of Structural Engineering, Peter Jordan Street 82, 1190 Vienna, Austria*
[b] *Tun Abdul Razak Research Centre, MRPRA, Brickendonbury, Hertford, UK*
[c] *Department of Mathematics, University of Glasgow, Glasgow G12 8QW, UK*

Abstract

In this paper we examine the change in material response, in particular the dilatational response, due to cavitation damage arising from tensile hydrostatic stresses of sufficient magnitude. A general discussion of stress softening and cavitation is followed by a description of some new experimental results concerning the change in response in hydrostatic tension or compression or in shear due to cavitation damage. In hydrostatic tension there is a progressive reduction in the value of the tensile bulk modulus of the material during loading and significant stress softening on unloading. As a result of the cavitation damage the tensile bulk modulus in the natural configuration is reduced. Ultimately, failure of the material occurs at sufficiently large hydrostatic tension, typically when the volume increase locally exceeds a critical value, of the order of 2–3%. However, the compressive bulk modulus is unaffected by the cavitation damage. Moreover, it is also found that the shear modulus is likewise unchanged by cavitation. The experimental data are used to develop a theoretical model, based on the concept of pseudo-elasticity, to describe these phenomena. Specifically, the dilatational part of the strain-energy function of an elastic material depends on a damage parameter which provides a means for switching the form of the strain-energy function, thereby reflecting the stress softening associated with unloading. A good correspondence between the theory and the data is obtained.

Keywords: Shear; Compressive; Stress softening; Cavitation damage

1. Introduction

When rubberlike materials are subjected to repeated loading and unloading to a fixed strain amplitude the relationship between stress and strain is, in general, noticeably different in loading and unloading. In particular, in a simple tension test, for example, the stress on unloading is less than that on loading at the same value of strain. This effect is known as *stress softening*. Stress softening may be associated with the

* Corresponding author. Fax: +43-1-47654-5292.
E-mail addresses: dorfmann@mail.boku.ac.at (A. Dorfmann), fuller@rubber.demon.co.uk (K.N.G. Fuller), rwo@maths.gla.ac.uk (R.W. Ogden).

Mullins effect (see e.g. Mullins (1947), Mullins and Tobin (1957), Mullins (1969)), which is evident when a virgin specimen of material is first deformed to a given strain level (pre-conditioning) or, subsequently, in loading/unloading cycles for strains up to the fixed level. Most experimental studies of the Mullins effect focus on uniaxial tension; however, similar stress softening effects have been noticed in periodic compressive tests by Bergström and Boyce (1998), in oscillatory shear tests by Ernst and Septanika (1999) and, recently, in cyclic torsion tests by Sedlan (2000). These stress-softening phenomena are in general associated with the fracture or slip of relatively weak secondary bonding of the polymer chains and the filler particles.

The main part of the paper (Sections 2 and 3), however, will be concerned with stress softening in rubberlike solids associated with *cavitation damage*. This is evidenced by a reduction in the bulk modulus as a result of increases in volume. During cyclic testing, a critical state may be reached where microcavities suddenly grow inside the rubber, possibly initiated at sites of internal imperfections. Microscopic observations suggest that rubberlike solids contain cavities with a wide range of sizes, and these will tear open to form running cracks when the maximum extensibility of the rubber is reached. Some new experimental results are reviewed in Section 4 to illustrate the shear, compressive and dilatational response of unfilled rubber subjected to cavitation damage. One feature of the results is the observation that the bulk modulus of the material in hydrostatic tension reduces progressively after some critical value of the hydrostatic tension has been exceeded. The material is now permanently damaged and, after unloading, it is seen that the tensile bulk modulus (but not the compressive bulk modulus) in the unloaded configuration is changed. It is also found that the shear modulus is unchanged after the cavitation damage has occurred.

In Section 5, a theory of *pseudo-elasticity* is described and then used to model the change in the material response induced by cavitation damage. This is accomplished by incorporating into the elastic strain-energy function of an undamaged material an additional (*damage* or *softening*) variable, denoted η, associated purely with the volumetric part of the response. The inclusion of η provides a means of changing the form of the energy function during the deformation process. Since the cavitation damage is isotropic, a single variable η is sufficient to describe the softening process. Some concluding remarks are contained in Section 6.

2. Cavitation damage

It has long been known that rubber subjected to a hydrostatic tensile stress causes internal rupture known as cavitation; see for example, Gent (1990) and the references contained therein. Void nucleation and the growth of microcavities in natural rubber is a complex process that involves breakage of bonds in the polymer network, fracture of filler clusters and detachments of rubber chains from reinforcing particles. The purpose of this study is to focus on the experimentally observed loss of stiffness when rubber is subjected to cyclic hydrostatic tensile loading. In fact, a critical state may be reached when internal imperfections or cavities suddenly grow inside the rubber. Currently, we know little about these precursors. It is not clear if they are really submicroscopic bubbles, dust particle inclusions or possibly weakly cross-linked regions, but these microscopic material imperfections are the origin of bubble and crack formation when local hydrostatic tensile stresses larger than a material-dependent critical value are generated.

In spite of the importance that such phenomena play in fracture, crazing and other failure mechanisms, the behaviour of rubber subjected to hydrostatic tension has not received sufficient attention. The softening in the (hydrostatic) tension–volume response of rubber components may ultimately result in premature material failure. Typical applications in which stress levels sufficiently large to initiate cavitation may exist are multilayered elastomeric bearings where thin rubber layers are highly restrained by steel plates; see, for example, Burtscher and Dorfmann (1999) and Dorfmann and Burtscher (2000). Depending on the particular application, such plates may be subjected to bending or tilting, as discussed by Gent and Meinecke (1970).

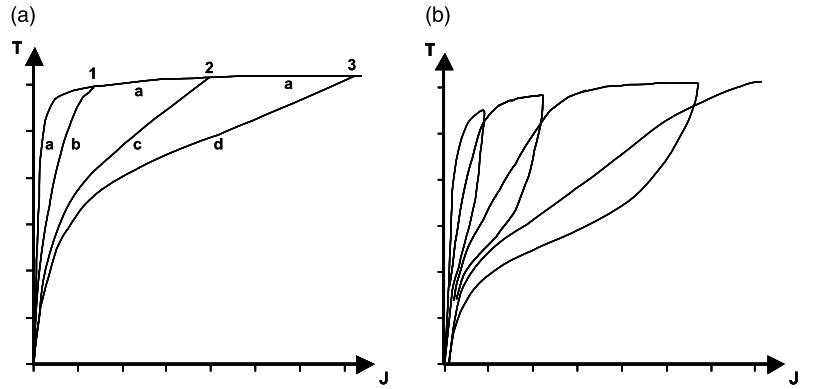

Fig. 1. Tension–volume relationship with cavitation: (a) idealized cavitation damage response; (b) typical experimental cavitation results for rubber.

A review of cavitation in nonlinearly elastic solids has been provided by Horgan and Polignone (1995) who describe cavitation as a bifurcation problem for a sphere of isotropic (or anisotropic) material under hydrostatic tension. In this work an explicit equation for the critical tension at which an internal cavity may be initiated is obtained. Their work relates to an earlier study by Ball (1982) in which, for a neo-Hookean material (incompressible), the critical tension is found to equal $5E/6$, where $E = 3G$ is Young's modulus in the natural configuration of the material, G being the shear modulus.

Consider a rubber specimen, in the shape of a cube say, subjected to uniform cyclic tensile loading on its boundary. Fig. 1(a) shows the idealized tension–volume response for unfilled natural rubber and Fig. 1(b) typical experimental results (see, for example, Kakavas and Chang (1991)). Let the loading procedure in Fig. 1(a) start with a stress-free fully unloaded specimen. The initial loading corresponds to the linear tension–volume response characterized by an elastic undamaged bulk modulus along path **a**. It will be shown in this section that a volume increase of 0.1% creates a critical hydrostatic tension in the material sufficient to initiate growth of microcavities and a subsequent reduction in the bulk modulus of the material. This is evidenced in Fig. 1(a) by a reduction in the slope of path **a**.

If unloading is initiated at a point **1**, for example, the equilibrium tension states during unloading are located along path **b**. Upon complete unloading, the material is assumed to have no permanent set and to return to the stress-free state. Re-loading now follows the previous unloading path **b** up to the point **1**, beyond which the primary path **a** is rejoined and additional cavitation damage is generated as the slope reduces progressively to almost zero (so that ultimately the material can support no further increase in tension). The tension–volume equilibrium states remain located on path **a** until a new unloading path is initiated at point **2**. The material memorizes the maximum volumetric dilatation it has seen; if subsequent cyclic volumetric changes remain below this threshold, no additional damage is accumulated in the material. The damage may be described as a progressive deterioration of the bulk stiffness in the material, as exemplified by the loading/re-loading paths **a**, **b**, **c** and **d**.

3. Hydrostatic loading of rubber

The shear modulus of natural rubber varies with temperature and strain from approximately 0.5–6.0 MPa. On the other hand, the bulk modulus is in general assumed to be strain independent and typically has values between 2000 and 3000 MPa depending on the vulcanizate and temperature. Because of the high ratio of bulk to shear modulus rubber is often treated as an incompressible material. Numerical results

based on use of fully incompressible material models give good accuracy for applications involving plane stress states such as those arising in shells or membranes (e.g. inflation of a balloon). However, if the material is highly constrained, as might be the case in a plane strain configuration of a thick body, the incompressibility assumption can be problematic, and the assumption of strict incompressibility must be relaxed by inclusion of a dilatational term in the strain-energy function, as discussed by, for example, Peng and Chang (1997).

This is the case, for example, in multilayered elastomeric bearings, where the pressure–volume relation of the material must be accounted for in order to obtain realistic results. In Fig. 2 the cross-section of a single rubber layer constrained by steel plates on its upper and lower surfaces under plane strain conditions is shown. The deformed shapes and the corresponding states of stress on the free edges and in the centre region are indicated schematically for both compressive and tensile loading. Because of the symmetry no out-of-plane deformation exists. On the free edges there are stress components in the loading and the out-of-plane directions, but the material is not constrained in the horizontal direction. This situation changes toward the centre, where the material is confined in all three directions and a positive or negative hydrostatic state of stress develops.

In compression the rubber can easily withstand high pressure without accumulation of damage. On the other hand, Gent (1990) has shown analytically that in hydrostatic tension internal cracking nucleated by precursors can expand to an indefinitely large size under a hydrostatic stress of approximately $5E/6$, where E is Young's modulus in the natural configuration. The initial size of the existing precursors has an important influence on the minimum cavitation stress. It was observed by Gent that small cavities are much more resistant to expansion and fracture than larger ones. For voids with diameter of the order of 0.5 μm pressures up to $3E$ are necessary to induce crack opening. Since microscopic voids with a wide range of sizes are always present, cavitation damage starts to develop at relatively low stress values. Initiation of cavitation damage is not visible from the outside but can be detected by a sudden drop in the load-extension curve or, in some cases, by audible cracking sounds.

Experimental results by Gent and Lindley (1958) showed that the critical stress for rupture is related to the elastic characteristics of the material and is independent of its strength properties. Taking advantage of the incompressibility of rubber, Gent and Tompkins (1969) were able to design a complementary method to confirm these findings. The work by Gent and Lindley (1958) formed the background for further experimental results obtained by Lindsey (1967). Using an approximate analytical solution, Lindsey quantified the value of the aspect ratio of the test specimen (diameter/thickness) for which the stress is essentially hydrostatic. This value depends on the compressibility of the material and increases as the material becomes more compressible. For example, for an almost incompressible material (Poisson's ratio about 0.49) a minimum aspect ratio of about 15 is required. See also the finite element study by Chang and Peng (1992).

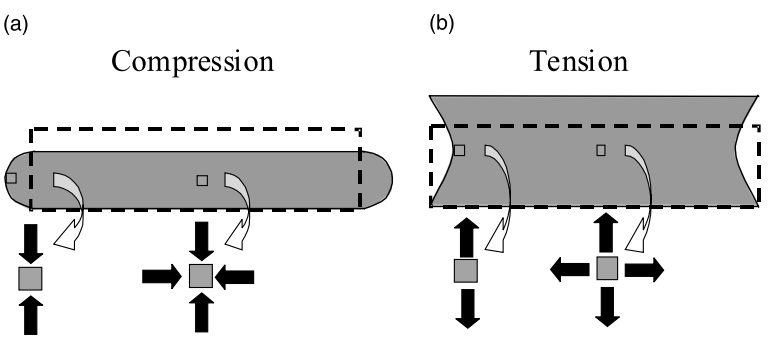

Fig. 2. Deformed shapes of a single rubber layer between two steel plates: (a) compression; (b) tension.

3.1. Cavitation tests using dissolved gases

In the method suggested by Gent and Tompkins (1969) soluble gas under high pressure was applied to rubber blocks so as to fill the internal microscopic voids. It was found that upon a sudden release of the gas pressure, the cavities within the rubber expanded. Because of the assumed incompressibility of the material, a pressure applied to the interior of the cavities has the same dilating effect as the application of an equivalent far field triaxial stress field. Gent and Tompkins were able to establish the existence of a critical pressure P_c for the internal gas that is sufficient to cause submicroscopic voids to expand, this value depending upon the initial size. They showed that the value of P_c is extremely large for small voids, having radii in the order of 1–10 Å, but that it approaches the lower limit of $5G/2$ for cavities with initial radius of the order of 10^{-7} m. In other words, the minimum supersaturation pressure of a dissolved gas required to form visible bubbles is $5G/2$. These openings will be filled when gas is dissolved in the rubber. When the external pressure is then suddenly released, the internal gas pressure will inflate the bubbles. The kinetics of expansion is complicated by, among other factors, the surface energy of rubber, the diffusion coefficient, the solubility of gas in rubber and the material properties. As the bubbles expand in volume, the inside pressure reduces and diffusion into the cavity will eventually occur, thereby providing a means of relieving the supersaturation pressure in the specimen. In laboratory applications, the voids do not expand indefinitely because of the limited supply of gas in the rubber specimen and because of diffusion of the gas outward through the sides of the rubber block.

Trial end error experimental analysis provided upper and lower bounds on the supersaturation pressure that initiates bubble formation. The necessary minimum cavitation pressure was determined by an experimental arrangement that created a linear pressure gradient through a rubber specimen. On two opposite sides of the rubber sample different gas pressures were applied for a sufficient period of time to attain pressure equilibrium. After the sudden release of the pressure on both sides, bubbles started to form on one side of the specimen only. The pressure in the transient region was determined based on a linear variation between the two applied end values and the minimum pressure value P_c was determined as approximately $5G/2$.

To validate the critical conditions for bubble formation different pressures were applied to compounds characterized by different values of G. The lowest gas pressure for bubble formation was in good agreement with the $5G/2$ value found previously. For many compounds, however, no bubbles appeared even at substantially higher pressures. This might be explained by the absence of initial cavities of 10^{-7} m or larger. Similar findings were reported in later studies by Cho and Gent (1988) and Gent and Wang (1990).

4. New experimental results

New insight into cavitation damage and the progressive deterioration of the bulk stiffness was recently obtained by performing a sequence of tests on thin unfilled rubber discs cured at 140 °C. The experiments were conducted in the TARRC laboratory on single and double rubber discs bonded between rigid plates and subjected to a sequence of different loading conditions. The question of interest was if and how a change in the tension–volume behaviour influences the shear and compressive response.

Each rubber disc in Fig. 3 has a diameter of 50 mm and an initial thickness of 1.7 mm. These dimensions were selected in order to create an effective state of hydrostatic stress in the central part of the disc whenever the specimen is subjected to tensile or compressive loading, as discussed in Section 3. The lateral strains in the central region of the disc are vanishingly small and the deformation can therefore be regarded as approximately uniaxial *in this region*.

Sequences of shear, compression and tension tests were performed using a screw-driven testing machine at the TARRC laboratory. The head speeds for the tests were 2 mm/min for the double shear test (1),

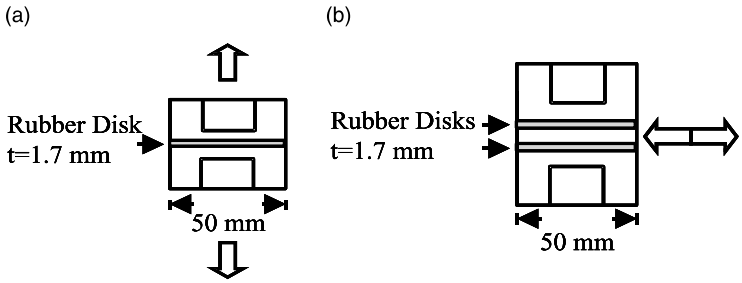

Fig. 3. Test configuration for (a) uniaxial tension or compression and (b) double shear.

0.4 mm/min for the compression test (2), 0.2 mm/min for the three cycles of the tension test below the cavitation stress (3), and 0.4 mm/min for the other tension tests (4). These specifications are summarized in Table 1.

Table 1 summarizes the initial material characterization tests (1–3) performed on the rubber discs to determine the material response before any accumulation of cavitation damage. The specimens were subjected to three loading–unloading cycles in double shear up to a maximum strain of 100%. Next, each of the specimens was subjected to three cycles in compression up to a maximum load of 20 kN and finally three loading–unloading cycles in tension with a maximum applied load just below the initial cavitation stress (which is approximately $5G/2$). The test results are shown in Fig. 4.

While in the central region of the disc the stress is effectively hydrostatic, this is certainly not the case towards the edges of the specimen. This means, in particular, that the load distribution over the plates is initially highly nonuniform. Hence, in tension for example, the hydrostatic stress in the central region is not given by the resultant normal load on a plate divided by the area of the plate. The latter ratio underestimates significantly the hydrostatic stress in this region. The slopes of the loading curves in the uniaxial tensile test shown in Fig. 4 do not therefore give the correct value of the bulk modulus of the material. The slope is approximately 250 MPa, which is an order of magnitude lower than the actual bulk modulus for this material.

The shear test results in Fig. 4 show typical curves associated with the response of unfilled natural rubber. Specifically there is some initial stress softening associated with the Mullins effect followed by loading–unloading cycles with small hysteretic loops and some residual strains. The shear stiffness is estimated from the linear portion of the third loading curve as 1.11 kN/mm, as indicated in Table 2.

Table 1
Test sequence and type for cavitation damage characterization

Test	Test type	Test specification	Head speed (mm/min)
1	Double shear test	3 cycles to 100% shear strain	2
2	Compression test	3 cycles to 20 kN	0.4
3	Tension test	3 cycles below cavitation stress (2 kN tensile force)	0.2
4	Tension test	3 cycles above cavitation stress (nominal 6% strain)	0.4
5	Double shear test	3 cycles to 100% shear strain	2
6	Compression test	3 cycles to 20 kN	0.4
7	Tension test	3 cycles above cavitation stress (nominal 50% strain)	0.4
8	Double shear test	3 cycles to 100% shear strain	2

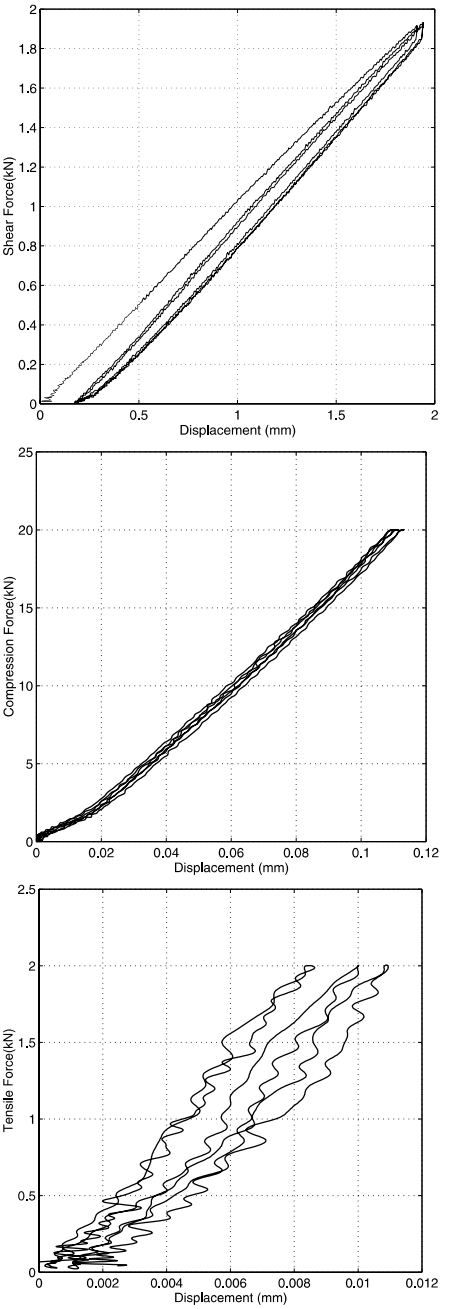

Fig. 4. Initial material characterization tests.

The results for compressive loading do not reveal any Mullins effect or residual strain and the hysteretic effects are not evident because of the small strains compared with those for shear. For future reference, the compressive stiffness is evaluated for the linear portion of the third loading curve as 189 kN/mm (see Table 2).

Table 2
Quantitative evaluation of the effect of cavitation on stiffness parameters

Test	Type of stiffness	Load range (3rd cycle)	Stiffness value
1	Shear stiffness	250–1750 N	1.11 kN/mm
2	Compression stiffness	5–15 kN	189 kN/mm
3	Tension stiffness	(Best line)	217 kN/mm
4	Tension stiffness	N.A.	N.A.
5	Shear stiffness	250–1750 N	1.14 kN/mm
6	Compression stiffness	5–15 kN	189 kN/mm
7	Tension stiffness	N.A.	N.A.
8	Shear stiffness	250–1750 N	1.09 kN/mm

The undamaged stiffness for tensile loading is determined using the best fit straight line and the result is 217 kN/mm. The oscillating nature of the curves is due to the extremely small displacement increments. Particular care was taken not to induce void growth and associated damage so as to provide a set of reference values for the undamaged material in shear, compression and tension. It should be noted that the initial slopes of the compression and tension curves approximately coincide. The tensile loading was then increased to generate almost 6% nominal axial strain in the material and a corresponding state of hydrostatic tension sufficient to initiate growth of microscopic cavities inside the rubber. The rapid change in slope of the force–displacement curve for the first loading in tension is apparent in Fig. 5. Upon unloading, the material response reflects the stress softening due to cavitation damage. Further, it is noted that this damage is not recovered and the initial slopes of the reloading curves are smaller than that of the original loading curve. This indicates a permanent reduction in the tensile bulk modulus due to damage.

Following the tensile test, the double shear and compression tests were then repeated in order to determine if cavitation damage influenced the response in shear or compression. The result are shown in Fig. 5 and comparison with Fig. 4 does not indicate any change.

During the third and final tensile test, the load is increased to generate 50% nominal strain so that the damage propagates to a larger part of the rubber specimen. Fig. 6 shows that the damage is irreversible and the bulk modulus reduces substantially when the material enters further into the critical region. The tensile force versus displacement curve in Fig. 6 also shows that the material has essentially failed and that no higher load can be supported. It is noted that the slope of the first tensile loading curve in Fig. 6 coincides with that of the reloading curves of the previous tension test (see Fig. 5). Also, in Fig. 6, results for subsequent double shear tests are shown. These confirm the earlier finding that the shear response is independent of cavitation.

The values of the stiffnesses and the applied load range within which each stiffness has been determined are summarized in Table 2. These indicate clearly that cavitation damage does not affect the shear modulus or the compressive bulk modulus. We believe that this is an important finding.

The results for tension can be seen more clearly in Fig. 7, where the curves for the different loading sequences are superimposed for comparison. The different horizontal scales of the two figures should be noted.

5. A pseudo-elastic model for cavitation damage

5.1. Hyperelasticity

We consider first a multiplicative decomposition of the deformation gradient $\mathbf{F}$ into a volume-changing (dilatational) and a volume-preserving (isochoric) part in the form

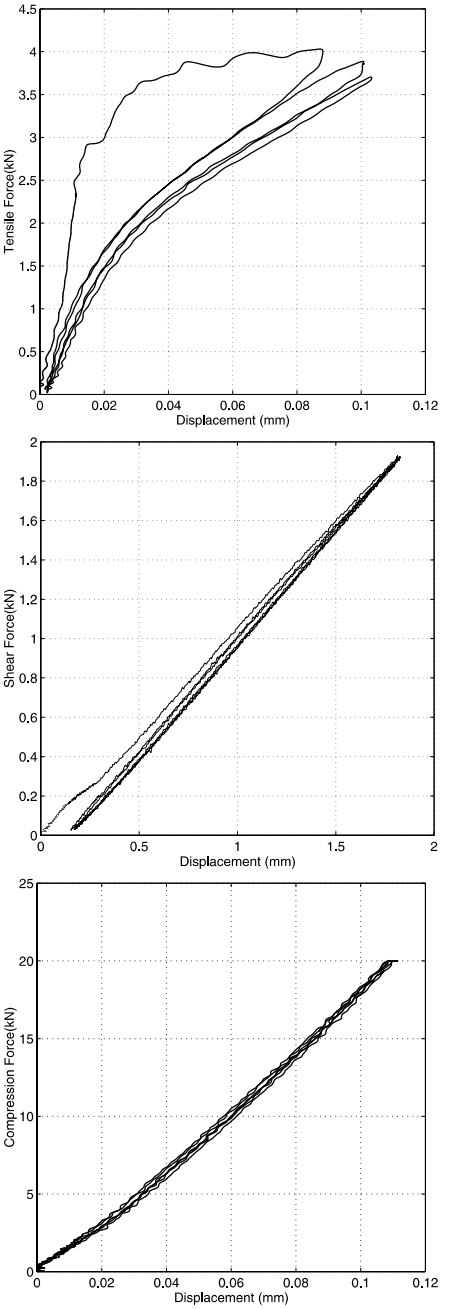

Fig. 5. Material characterization after initial cavitation damage.

$$\mathbf{F} = (J^{1/3}\mathbf{I})\overline{\mathbf{F}} = J^{1/3}\overline{\mathbf{F}}, \tag{1}$$

following Flory (1961) and Ogden (1976, 1978). The modified deformation tensor $\overline{\mathbf{F}}$ describes the volume-preserving part of the deformation, while the dilatational part is given in terms of the determinant

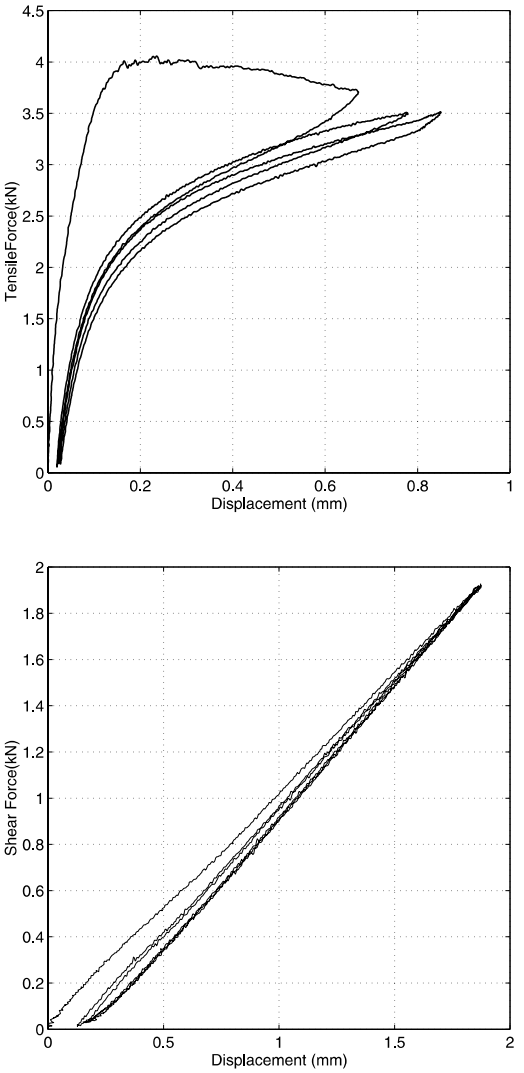

Fig. 6. Material shear response after further cavitation damage.

$J = \det \mathbf{F}$. It follows from (1) that

$$\det \overline{\mathbf{F}} = 1. \tag{2}$$

We denote by λ_i, $i = 1, 2, 3$, the principal stretches of the deformation and the modified principal stretches $\bar{\lambda}_i$, $i = 1, 2, 3$, are defined by

$$\bar{\lambda}_i = J^{-1/3}\lambda_i. \tag{3}$$

It follows that

$$\bar{\lambda}_1\bar{\lambda}_2\bar{\lambda}_3 = 1. \tag{4}$$

Here, we consider the material to be isotropic and elastic, so that the strain-energy function is a symmetric function, $W(\lambda_1, \lambda_2, \lambda_3)$ say, of the principal stretches.

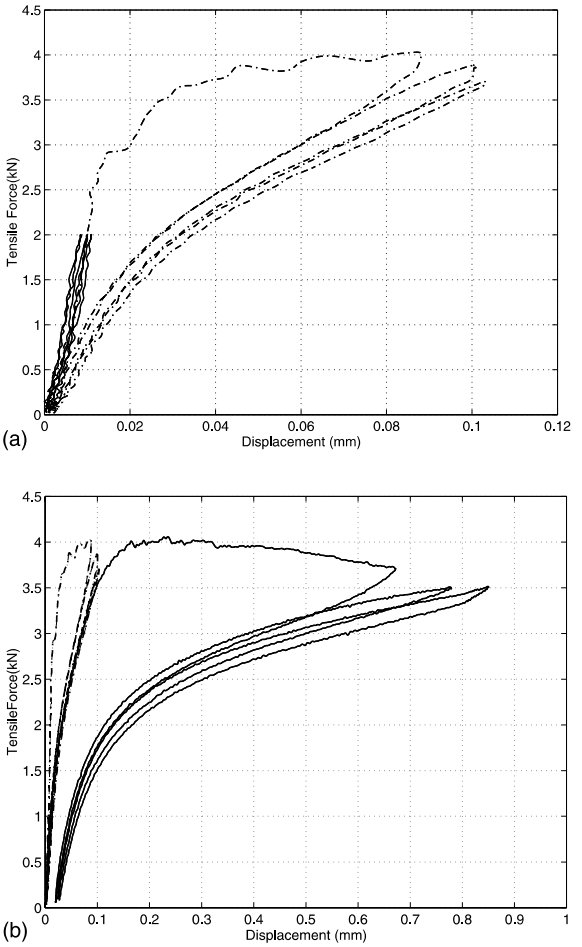

Fig. 7. Comparison of tensile load–displacement curves for undamaged and damaged material: (a) first and second test sequences; (b) second and third test sequences. In each case the dashed curves correspond to the second test sequence.

In order to separate the dependence of W into the isochoric and dilatational parts of the deformations, we regard it as a function of $\bar{\lambda}_1, \bar{\lambda}_2, \bar{\lambda}_3$ and J subject to (4), and we write

$$\overline{W}(\bar{\lambda}_1, \bar{\lambda}_2, \bar{\lambda}_3, J) = W(\bar{\lambda}_1 J^{1/3}, \bar{\lambda}_2 J^{1/3}, \bar{\lambda}_3 J^{1/3}), \tag{5}$$

which defines the notation $\overline{W}$. The principal Cauchy stresses σ_i are then given by

$$J\sigma_i = \bar{\lambda}_i \frac{\partial \overline{W}}{\partial \bar{\lambda}_i} - \bar{p}, \tag{6}$$

where $\bar{p}$ is defined by

$$\bar{p} = \frac{1}{3} \sum_{j=1}^{3} \bar{\lambda}_j \frac{\partial \overline{W}}{\partial \bar{\lambda}_j} - J \frac{\partial \overline{W}}{\partial J}. \tag{7}$$

The hydrostatic part of the stress is given simply by

$$\frac{1}{3}(\sigma_1+\sigma_2+\sigma_3)=\frac{\partial\overline{W}}{\partial J}. \tag{8}$$

For a purely hydrostatic tension T we have

$$\sigma_i=T=\frac{\partial\overline{W}}{\partial J},\quad i=1,2,3. \tag{9}$$

For the special case in which W is decoupled into dilatational and volume-preserving parts we write

$$W(\lambda_1,\lambda_2,\lambda_3)=\overline{W}(\bar{\lambda}_1,\bar{\lambda}_2,\bar{\lambda}_3,J)=W_{\mathrm{vol}}(J)+W_{\mathrm{iso}}(\bar{\lambda}_1,\bar{\lambda}_2,\bar{\lambda}_3), \tag{10}$$

where $W_{\mathrm{vol}}(J)$ and $W_{\mathrm{iso}}(\bar{\lambda}_1,\bar{\lambda}_2,\bar{\lambda}_3)$ respectively are the volumetric and volume-preserving parts of the energy.

Over the last 30 years extensive research has been conducted into the development of constitutive laws for both incompressible and compressible elastic materials, but to the best of the authors' knowledge there is no formulation currently available in the literature that accounts for the nonlinear tension–volume response due to cavitation damage. This may be due to the assumption of incompressibility frequently used for the analysis of rubber. However, the experimental evidence discussed in Section 4 indicates clearly that incompressibility is not appropriate, and, when the material is subject to hydrostatic tensions beyond a critical value, neither is a linear tension–volume response.

We propose first to derive an expression for the volumetric part $W_{\mathrm{vol}}(J)$ of the strain energy, the first derivative of which gives the hydrostatic pressure in accordance with Eq. (8). This is depicted schematically by the curve **a** in Fig. 1. The second derivative is the bulk modulus. For an increase in volume ($J>1$) it is important that the strain energy function takes into account the growth of microcavities and fracture of weak junctions in polymer chains. Failure of physical links and growth of cavities manifest themselves in the reduction of the tension–volume stiffness at the macroscopic level (see Figs. 5 and 6). Secondly, to include the noticeable difference in the dilatational response during loading and unloading (stress softening) we propose to use different elastic formulations that reflect the accumulated damage in the material.

5.2. Pseudo-elasticity

The development is based on the pseudo-elasticity theory developed by Ogden and Roxburgh (1999a,b) and Ogden (2000, 2001), in which the material response is described by different forms of strain-energy function on primary loading and subsequent unloading. The starting point of this approach is the compressible isotropic theory of hyperelasticity outlined above. An additional single scalar damage parameter η is incorporated as a means of modifying the energy function. For the decoupled strain-energy function (10), η is included only in the volumetric part, and the resulting *pseudo-elastic energy function* is written

$$W(\lambda_1,\lambda_2,\lambda_3,\eta)=W_{\mathrm{vol}}(J,\eta)+W_{\mathrm{iso}}(\bar{\lambda}_1,\bar{\lambda}_2,\bar{\lambda}_3). \tag{11}$$

During the deformation process the parameter η may be either active or inactive and may switch from inactive to active and conversely provided it remains continuous in so doing. When it is inactive, the material behaves as an elastic material described by a dilatational strain energy function $W_{\mathrm{vol}}(J,\eta)$, where η is held constant. Without loss of generality, we set this value equal to one and define for the initial (hydrostatic) loading from an unstressed configuration of an undamaged material through the dilatational part

$$\widetilde{W}_{\mathrm{vol}}(J)=W_{\mathrm{vol}}(J,1) \tag{12}$$

of the strain energy, where the superposed tilde refers to primary loading path. The first derivative of this expression gives the tension–volume response

$$\widetilde{T}(J)=\frac{\mathrm{d}\widetilde{W}_{\mathrm{vol}}}{\mathrm{d}J}(J) \tag{13}$$

for a perfectly elastic material for which the primary loading path is also the unloading path.

On the other hand, when η is active it is determined implicitly in terms of J by the constraint equation

$$\frac{\partial W_{\text{vol}}}{\partial \eta}(J,\eta) = 0. \tag{14}$$

Under appropriate conditions this equation is equivalent to writing the damage parameter η as a function of the volumetric change J in the form $\eta = \chi(J)$. The material properties are again described in terms of a strain-energy function, but with its volumetric part given by $W_{\text{vol}}(J, \chi(J))$ instead of $W_{\text{vol}}(J, 1)$.

Standard energy functions given by, for example, Ogden (1972), Simo and Pister (1984) or Simo and Miehe (1992) cannot be used as representative of $\widetilde{W}_{\text{vol}}(J)$ since they do not include the stress softening effect attributed to cavitation damage. However, the requirements that $\widetilde{W}_{\text{vol}}(J)$ has a global minimum of 0 at $J = 1$ and that $\widetilde{W}_{\text{vol}}(J)$ is an increasing function of J are applicable.

It is assumed that unloading from any point along the primary loading path activates η, which is then given in terms of J during unloading by Eq. (14). We write the resulting volumetric part of the strain energy for unloading and subsequent submaximal loading and unloading paths as

$$\overline{W}_{\text{vol}}(J) = W_{\text{vol}}(J, \chi(J)) \tag{15}$$

and the corresponding tension as

$$\overline{T}(J) = \frac{\mathrm{d}\overline{W}_{\text{vol}}}{\mathrm{d}J}(J) = \frac{\partial W_{\text{vol}}}{\partial J}(J, \chi(J)). \tag{16}$$

The damage parameter η is expressed in terms of the deformation to provide both an evolution equation for the damage and a means of modifying the strain-energy function. Thus, for consistency with Eqs. (12) and (15), at the point where unloading is initiated from the virgin (primary) loading path, the maximum value of J is denoted $J_{\max}$ and $\chi(J_{\max})$ assumes the value 1. This implies that the function χ and hence $W_{\text{vol}}(J, \chi(J))$ depends on the point from which unloading starts.

Following the work of Ogden and Roxburgh (1999a,b), specialized to the volumetric part of the energy function, we adopt a pseudo-energy function for the tension–volume response in the form

$$W_{\text{vol}}(J,\eta) = \eta \widetilde{W}_{\text{vol}}(J) + \phi(\eta), \tag{17}$$

where $\phi(\eta)$ is referred as a *damage function*, which, for consistency, vanishes during primary loading, i.e. when $\eta = 1$. Thus,

$$\phi(1) = 0. \tag{18}$$

During primary loading, the tension $\widetilde{T}(J)$ is given by Eq. (13). For unloading and subsequent submaximal cyclic loading the tension is

$$T(J) = \eta \frac{\mathrm{d}\widetilde{W}_{\text{vol}}}{\mathrm{d}J}(J) = \eta \widetilde{T}(J). \tag{19}$$

Eq. (14), when applied to (17), yields the connection

$$\widetilde{W}_{\text{vol}}(J) + \phi'(\eta) = 0 \tag{20}$$

between η and J, where the prime indicates differentiation with respect to η. At the initiation of unloading Eq. (20) gives

$$\phi'(1) = -\widetilde{W}_{\text{vol}}(J_{\max}) \equiv -W_{\max}, \tag{21}$$

wherein the notation $W_{\max}$ is defined.

The function ϕ is also required to satisfy the condition $\phi''(\eta) < 0$. As a result, when the material is unloaded, i.e. not subjected to any volumetric change ($J = 1$), η will assume its minimum value, $\eta_{\min}$ say, such that

$$\phi'(\eta_{\min}) = -\widetilde{W}_{\mathrm{vol}}(1) = 0. \tag{22}$$

Since the function ϕ depends on the point where unloading begins then so does $\eta_{\min}$, that is, it depends through $W_{\max}$ on the value $J_{\max}$.

The selection of $\phi(\eta)$ is subject to the above constraints and serves to determine the damage parameter η in terms of the volumetric deformation J through Eq. (20). For a more detailed discussion on the subject of pseudo-elasticity, we refer to Ogden and Roxburgh (1999a,b) and Ogden (2000, 2001).

5.3. Comparison of experimental and numerical data

The theory described in Sections 5.1 and 5.2 applies *locally* or, in the case of a homogeneous deformation, to the overall response of the body. In the experiments discussed in Section 4, however, the deformation is not homogeneous and it is not a straightforward matter to derive expressions for the overall force–displacement response from the local stress–strain relations such as Eqs. (13) and (14).

To circumvent this problem, we consider the response to be that of an *equivalent homogeneous material* for which the deformation is homogeneous. In particular, for this purpose, we focus here on the tensile response, in which the local relation (13) is replaced by an overall counterpart, written

$$T^*(J^*) = \frac{\mathrm{d}W^*_{\mathrm{vol}}}{\mathrm{d}J^*}(J^*), \tag{23}$$

where T^* is the total applied force on the plate per unit area, J^* is a measure of the overall volume change in the cylindrical specimen subject to homogeneous uniaxial extension. It is equal to the ratio of the current to the initial thickness of the specimen. The term $W^*_{\mathrm{vol}}(J^*)$ is the volumetric part of total stored energy per unit initial volume, and is equal to the mean value of $\widetilde{W}_{\mathrm{vol}}(J)$ over the actual volume of the specimen. Analogous expressions can be given for the overall counterparts of the other equations in Sections 5.1 and 5.2, but we do not list these separately. We emphasize that J^* and the overall counterpart of η are uniform for this equivalent homogeneous material. In a numerical analysis, based on, for example, the finite element method, J and η are nonhomogeneous and the pseudo-energy function applies locally. This would enable a detailed analysis of the size of the damaged zone to be conducted, but this is not our objective here.

Our aim now is to develop a particular model for W^*_{vol} capable of describing the (overall) tension–volume response of the thin rubber discs shown in Fig. 3.

As mentioned earlier, the dimensions of the test specimens were selected in order to ensure a hydrostatic state of stress with three equal principal stresses during uniaxial loading. For the equivalent homogeneous deformation the three principal stresses are approximately equal to T^*. Thus, effectively, lateral stresses are needed to ensure the homogeneity. The uniaxial stress–strain tensile data can therefore be viewed as equivalent to hydrostatic tension–volume data suitable for the characterization of the volumetric part of the strain-energy function. The volume changes have been calculated from the experimental data with the edge effects neglected. The errors in this approximation are negligible because the aspect ratio used in the experiments is about 30.

The choice of the function $W^*_{\mathrm{vol}}(J^*)$ is arbitrary, subject to the usual requirements that it has an absolute minimum at $J^* = 1$ and that its first derivative gives the tension–volume response. Its second derivative gives the bulk modulus of the equivalent homogeneous material. As we see below, this is an order of magnitude lower than the actual bulk modulus, which, we recall, is given by the second derivative of $\widetilde{W}_{\mathrm{vol}}(J)$ with respect to J.

To describe the pressure–volume relation during the initial loading process, we propose to use the error function with two material parameters m^* and κ^* such that the dilatational strain-energy can be expressed as

$$W^*_{\mathrm{vol}}(J^*) = m^*\kappa^* \int_1^{J^*} \mathrm{erf}\left[\frac{1}{m^*}(J-1)\right] \mathrm{d}J, \tag{24}$$

where κ^* is the bulk modulus described above for the material in the natural configuration before any damage occurs. The tension–volume relation is then

$$T^*(J^*) = m^*\kappa^* \mathrm{erf}\left[\frac{1}{m^*}(J^*-1)\right]. \tag{25}$$

The parameter m^* provides enough flexibility to enable the bulk modulus to be changed gradually from its initial value κ^* to essentially zero, as shown below. It is emphasized that this expression represents the overall material response only for the initial monotonic loading process, as indicated schematically by curve **a** in Fig. 1. A nonlinear least squares method can be used to determine the value of the parameter m^* with a suitable degree of accuracy in order best to fit the data.

In order to compare the theory with the available test results, we consider the uniaxial test data shown in Fig. 5 and, for convenience, convert the data into tension–volume results. An appropriate value of κ^* is about 154 MPa (which compares with a value of 2360 MPa for bulk modulus of the actual material), while a suitable value of the parameter m^* is 0.013. The experimental and numerical data are shown in Fig. 8. Fair agreement is demonstrated between experimental data and the results of the numerical simulation. Fig. 8 shows that upon unloading a different path is followed and thus a modified strain-energy function needs to be determined in order to describe the accumulated damage in the material. This is accomplished by introducing the scalar damage parameter η^*, as for η in Eq. (17). In view of the interpretation given above, it is no longer appropriate to view $W^*_{\mathrm{vol}}(J^*, \eta^*)$ as a stored energy function. The term pseudo-energy function is preferred.

The damage function, now denoted ϕ^*, serves to determine the damage parameter η^* and can be selected arbitrarily subject to the constraints on ϕ identified in Section 5.2. Furthermore, from Eq. (19) it is evident that η^* must satisfy the inequalities $0 < \eta^* \leqslant 1$.

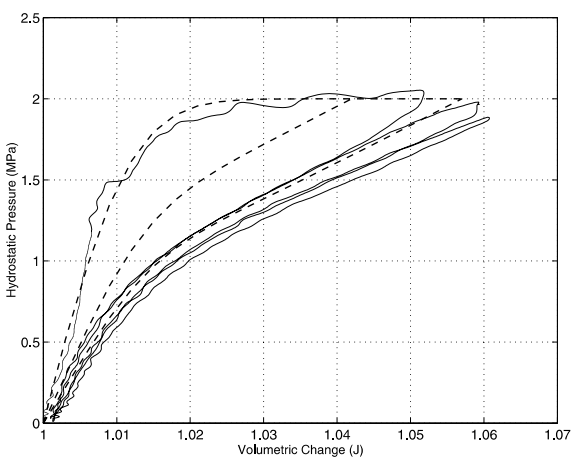

Fig. 8. Experimental and numerical pressure–volume response.

Let us assume that unloading starts at any arbitrary point along the primary loading path at which the value of J^* is $J^*_{\max}$. The accumulated energy is then given by $W^*_{\max} = -\phi^{*'}(1)$, analogously to Eq. (21). We choose the function $\phi^*(\eta^*)$ to describe stress softening in the form

$$\phi^{*'}(\eta^*) = -n\kappa^* \mathrm{erf}^{-1}[s^*(\eta^* - 1)] + W^*_{\max}, \tag{26}$$

where n^* and s^* are positive dimensionless material constants and erf^{-1} is the inverse of the error function. After rearrangement, we obtain η^* explicitly in the form

$$\eta^* = 1 - \frac{1}{s^*}\mathrm{erf}\left[\frac{1}{n^*\kappa^*}\left(W^*_{\max} - W^*_{\mathrm{vol}}(J^*)\right)\right]. \tag{27}$$

Since n^* and s^* are positive it follows that $\eta^* \leqslant 1$, with equality holding only when $W^*_{\mathrm{vol}}(J^*) = W^*_{\max}$. Finally, on use of (22), the minimum value $\eta^*_{\min}$ of η^* is given by

$$\eta^*_{\min} = 1 - \frac{1}{s^*}\mathrm{erf}\left(\frac{W^*_{\max}}{n^*\kappa^*}\right). \tag{28}$$

This value is positive for all $W^*_{\max} > 0$ and $n^* > 0$ if $s^* > 1$.

To validate the proposed formulation, the damage parameter η^* associated with the tension–volume unloading data shown in Fig. 8 is obtained, with a best fit corresponding to the parameter values $s^* = 1.01$ and $n^* = 0.022$.

6. Conclusions

The experimental results described in this paper highlight the progressive reduction in the value of the bulk modulus of the material during hydrostatic tensile loading and the significant stress softening that occurs during unloading from a state of hydrostatic tension. The ultimate failure of the material, which occurs at sufficiently large hydrostatic tension and typically when the volume increase locally is of the order of 3%, illustrates the caution that needs to be adopted when using constitutive laws for compressible elastic materials for engineering calculations, particularly in finite element calculations, in situations where there might be a large local hydrostatic tension. Moreover, there is a permanent reduction in the (hydrostatic) tensile stiffness of the material due to increased cavitation damage. On the other hand, not surprisingly, there is no change in the (hydrostatic) compressive stiffness. It is also found that the shear stiffness in the unstressed configuration is unchanged as a result of the cavitation.

The experimental data have been used as the basis for constructing a theoretical model to describe these effects. Specifically, we have focussed on the dilatational part of the strain-energy function of an elastic material. First, we obtained a form of this function which reflects the overall hydrostatic tension–volume response described above. Then, we used the notion of pseudo-elasticity, in which the dilatational part of the energy function depends on a damage parameter. This enables the form of the dilatational response to be changed when loading terminates and unloading is initiated, and thus reflects the stress softening associated with unloading. The theoretical model provides a good characterization of the experimental results described.

References

Ball, J.M., 1982. Discontinuous equilibrium solutions and cavitation in nonlinear elasticity. Phil. Trans. R. Soc. Lond. A 306, 557–610.

Bergström, J.S., Boyce, M.C., 1998. Constitutive modelling of the large strain time-dependent behavior of elastomers. J. Mech. Phys. Solids 46, 931–954.

Burtscher, S.L., Dorfmann, A., 1999. Experimental and computational aspects of cavitation in natural rubber. In: Dorfmann, A., Muhr, A. (Eds.), Proceedings of the First European Conference on Constitutive Models for Rubber. Balkema, Rotterdam.
Chang, W.V., Peng, S.H., 1992. Nonlinear finite element analysis of the butt-joint elastomer specimen. J. Adhesion Sci. Technol. 6, 919–939.
Cho, K., Gent, A.N., 1988. Cavitation in model elastomeric components. J. Mater. Sci. 23, 141–144.
Dorfmann, A., Burtscher, S.L., 2000. Aspects of cavitation damage in seismic bearings. J. Struct. Eng., ASCE 126, 573–579.
Ernst, L.J., Septanika, E.G., 1999. A non-Gaussian network alteration model. In: Dorfmann, A., Muhr, A. (Eds.), Proceedings of the First European Conference on Constitutive Models for Rubber. Balkema, Rotterdam.
Flory, P.J., 1961. Thermodynamic relations for high elastic materials. Trans. Farad. Soc. 57, 829–838.
Gent, A.N., 1990. Cavitation in rubber: a cautionary tale. Rubber Chem. Technol. 63, 49–53.
Gent, A.N., Lindley, P.B., 1958. Internal rupture of bonded rubber cylinders in tension. Proc. R. Soc. Lond. A 249, 195–205.
Gent, A.N., Meinecke, E.A., 1970. Compression, bending and shear of bonded rubber blocks. Polymer Eng. Sci. 10, 48–53.
Gent, A.N., Tompkins, D.A., 1969. Nucleation and growth of gas bubbles in elastomers. J. Appl. Phys. 40, 2520–2525.
Gent, A.N., Wang, C., 1990. Physics of rubber as related to the automobile. J. Appl. Phys. 9, 3392–3395.
Horgan, C.O., Polignone, D.A., 1995. Cavitation in nonlinearly elastic solids: a review. Appl. Mech. Rev. 48, 471–485.
Kakavas, P.A., Chang, W.V., 1991. Acoustic emission in bonded elastomer discs subjected to uniform tension. II. J. Appl. Polym. Sci. 42, 1997–2004.
Lindsey, G.H., 1967. Triaxial fracture studies. J. Appl. Phys. 38, 4843–4852.
Mullins, L., 1947. Effect of stretching on the properties of rubber. J. Rubber Res. 16, 275–289.
Mullins, L., 1969. Softening of rubber by deformation. Rubber Chem. Technol. 42, 339–362.
Mullins, L., Tobin, N.R., 1957. Theoretical model for the elastic behaviour of filler-reinforced vulcanized rubbers. Rubber Chem. Technol. 30, 551–571.
Ogden, R.W., 1972. Large deformation isotropic elasticity: on the correlation of theory and experiment for compressible rubberlike solids. Proc. R. Soc. Lond. A 328, 567–583.
Ogden, R.W., 1976. Volume changes associated with the deformation of rubber-like solids. J. Mech. Phys. Solids 24, 323–338.
Ogden, R.W., 1978. Nearly isochoric elastic deformations: application to rubberlike solids. J. Mech. Phys. Solids 26, 37–57.
Ogden, R.W., 2000. Elastic and pseudo-elastic instability and bifurcation. In: Petryk, H. (Ed.), Material Instabilities in Elastic and Plastic Solids CISM Courses and Lectures Series no. 414. Springer, Wien.
Ogden, R.W., 2001. Stress softening and residual strain in the azimuthal shear of a pseudo-elastic circular cylindrical tube. Int. J. Non-linear Mech. 36, 477–487.
Ogden, R.W., Roxburgh, D.G., 1999a. A pseudo-elastic model for the Mullins effect in filled rubber. Proc. R. Soc. Lond. A 455, 12861–12878.
Ogden, R.W., Roxburgh, D.G., 1999b. An energy-based model of the Mullins effect. In: Dorfmann, A., Muhr, A. (Eds.), Proceedings of the First European Conference on Constitutive Models for Rubber. Balkema, Rotterdam.
Peng, S.H., Chang, W.V., 1997. A compressible approach in finite element analysis of rubber-elastic materials. Comput. Struct. 62, 573–593.
Sedlan, K. 2000. Viskoelastic Materialverhalten von Elastomerwerkstoffen: Experimentelle Untersuchung und Modellbildung. Ph.D. Dissertation, University of Kassel.
Simo, J.C., Miehe, C., 1992. Associative coupled thermoplasticity at finite strains: formulation, numerical analysis and implementation. Comput. Meth. Appl. Mech. Eng. 98, 41–104.
Simo, J.C., Pister, K.S., 1984. Remarks on rate constitutive equations for finite deformation. Comput. Meth. Appl. Mech. Eng. 46, 201–215.